Fatigue & Fracture of
Engineering Materials & Structures

doi: 10.1111/j.1460-2695.2010.01502.x

Numerical analysis of the ENF and ELS tests applied to mode II fracture characterization of cortical bone tissue

M. F. S. F. de MOURA,[1] N. DOURADO,[2] J. J. L. MORAIS[2] and F. A. M. PEREIRA[2]

[1]Faculdade de Engenharia da Universidade do Porto, Departamento de Engenharia Mecânica e Gestão Industrial, Rua Dr. Roberto Frias, 4200-465 Porto, Portugal, [2]CITAB/UTAD, Departamento de Engenharias, Quinta de Prados, 5001-801 Vila Real, Portugal

Received in final form 25 May 2010

ABSTRACT The objective of this work is to verify numerically the adequacy of the ENF and the ELS tests to determine the fracture toughness under mode II loading of cortical bovine bone tissue. A data-reduction scheme based on the specimen compliance and the equivalent crack concept is proposed to overcome the difficulties inherent to crack monitoring during its growth. A cohesive damage model was used to simulate damage initiation and growth, thus assessing the efficacy of the proposed data-reduction scheme. The influences of the initial crack length, local strength and toughness on the measured fracture energy were analysed, taking into account the specimen length restriction. Some limitations related to spurious influence on the fracture process zone of the central loading in the ENF test, and clamping conditions in the ELS test were identified. However, it was verified that a judicious selection of the geometry allows, in both cases, a rigorous estimation of bone toughness in mode II.

Keywords bone; cohesive zone modelling; fracture characterization; mode II.

NOMENCLATURE

a = crack length
a_0 = initial crack length
a_e = equivalent crack length
B = specimen width
C = specimen compliance
C_0 = initial specimen compliance
E_f = corrected flexural modulus
E_L = longitudinal modulus
E_T = transverse modulus
G_I = strain energy release rate in mode I
G_{Ic} = fracture toughness in mode I
G_{II} = strain energy release rate in mode II
G_{IIc} = fracture toughness in mode II
G_{LT} = shear modulus
h = specimen height
L = specimen characteristic length
L_{ef} = effective length in the ELS test
P = applied load
δ = applied displacement
Δ_I = crack length correction
σ_i = stresses in each mode (i = I, II)
$\sigma_{u,i}$ = local strengths (i = I, II)

Correspondence: M. F. S. F. de Moura. E-mail: mfmoura@fe.up.pt

CBT = Corrected beam theory
CCM = Compliance calibration method
CZM = Cohesive zone model
ELS = End loaded split
ENF = End notched flexure
FEM = Finite element method
FPZ = Fracture process zone

INTRODUCTION

Fracture behaviour of cortical bone has attracted the attention of many researchers.[1–7] Effectively, the fracture of healthy bone tissue needs to be understood in order to predict and reduce fractures due to aging, exercise, over-use and disease. The key issue is to determine the toughness which represents the mechanical property that describes the bone resistance to crack initiation and propagation. Two parameters can be used to identify the toughness: the critical stress intensity factor (K_c) and the critical strain energy release rate (G_c). The K_c is a scaling factor that describes the alteration of stress state in the vicinity of the crack tip, whereas G_c measures the energy required to extend a pre-existing crack. One important difference between both is that K_c is a local parameter, whereas G_c represents a global variation of the structure energy when the pre-existing crack grows. Cortical bone is a heterogeneous composite material, with an anisotropic and complex hierarchical microstructure, comprising mineral (mainly hydroxyapatite), organic (mostly type I collagen) and water phases. Consequently, being a global parameter, G_c is more appropriate than K_c to measure toughness because K_c can be drastically affected by local variations of the internal material constitution. Alternatively, Yan *et al.*[8] proposed the J-integral to account for the plastic deformation of bone induced by several toughening mechanisms, e.g. microcracking, osteon pullout, fibre bridging and crack deflection. The authors concluded that the toughness of bone estimated using the J-integral is much greater than the toughness measured using the critical stress intensity factor. Yang *et al.*[9] proposed a cohesive model as a nonlinear fracture model in order to account for the damage zone developed in bone. They argue that linear elastic fracture mechanics is unable to account for the load-displacement curves shape but the nonlinear model overcomes this deficiency. Ural *et al.*[10] used cohesive finite element modelling to analyse the age-related toughness loss in human cortical bone. The authors concluded that cohesive models are able to capture and predict the parameters related to bone fracture by representing the physical processes occurring in the vicinity of a propagating crack. The majority of the works about fracture characterization of bone tissue are dedicated to mode I loading. The compact tension test[3] and the single-edge notched specimen under three-point bending[11] are commonly used. The difficulties associated in getting specimens with the required size lead to the employment of the single-layer compact sandwich specimen.[12] In this specimen a bone coupon was sandwiched between two holders of polymethylmethacrylate. Much less attention has been dedicated to fracture characterization under mode II loading which is justified by the difficulty of defining an adequate test. Norman *et al.*[13] proposed the compact shear test for mode II fracture characterization of human bone. Subsequently, Brown *et al.*[14] used the same test to evaluate fracture toughness dependency on bone location and age. However, this test presents three disadvantages: (1) small variation of compliance as a function of pre-crack length which turns difficult the establishment of compliance calibration; (2) mixed-mode crack growth instead of pure-mode II and (3) unstable propagation, which means that only crack initiation fracture toughness is available.

Fracture tests using bovine bone are frequently performed because it provides longer specimens relative to the human's. Norman *et al.*[3] reported that fracture toughness of human bone was lower than that of bovine. However, when normalized by their respective strengths, the two types of bone were equally tough, implying that the mechanisms which give higher strength may also be responsible for higher toughness. Although the fracture properties of bovine and human cortical bone are not equal,[14,15] the same kind of experimental test can be applied to determine those properties. This particularity can be used to identify new test methods using bovine cortical bone.

The objective of this work is to perform a numerical study on the mode II fracture characterization of bone. This work acquires special relevancy in the context of shear and mixed-mode (I + II) fractures. In reality, it is known that the majority of the bone fracture *in vivo* occurs under mixed-mode (e.g. I + II), which emphasizes the necessity to define adequate fracture criteria in the $G_I - G_{II}$ space. In this context, it is important to determine the fracture toughness under mode II loading. Thus, the applicability of the ENF and the ELS tests to mode II fracture characterization of bovine bone in the tangential-longitudinal (TL) fracture system (Figs 1 & 2) was numerically assessed. These tests are particularly suitable for mode II fracture characterization because of their simplicity and the possibility to use the beam theory to measure the fracture energy. They are frequently used

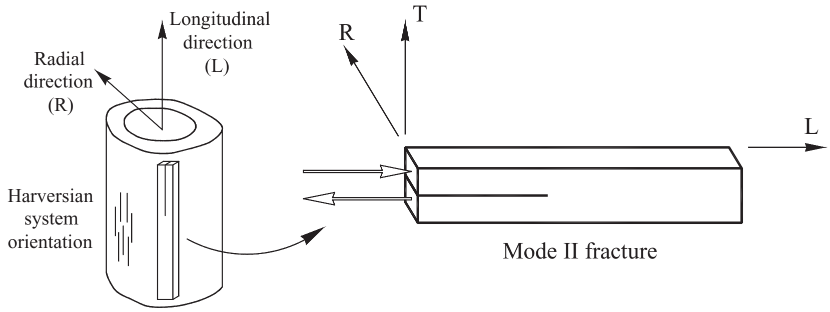

Fig. 1 Schematic diagram of the femur bone showing the location where samples can be harvested.

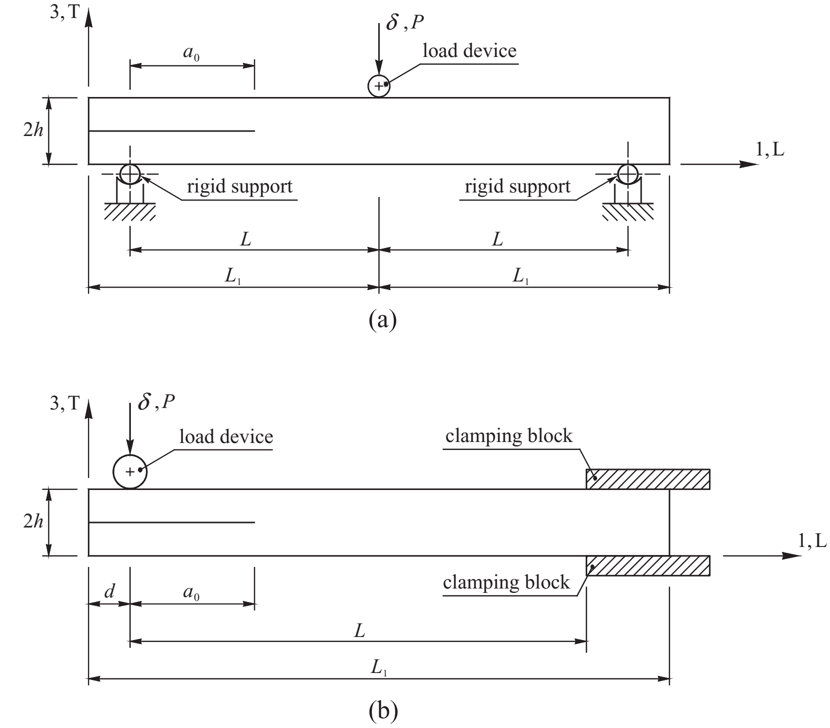

Fig. 2 Mode II test configurations. (a) ENF and (b) ELS.

to evaluate the fracture properties of different materials, e.g. wood,[16,17] composites[18] or bonded joints.[19,20] However, these fracture tests have never been applied to bone. Hence, the applicability of these tests in the context of bone fracture characterization requires a careful analysis owing to the limitations of producing adequate specimen sizes. Bone fracture in mode II exhibits a pronounced FPZ ahead of the crack tip due to several toughening mechanisms, which must not interact with the external loading or boundary conditions to assure self-similar crack propagation. This issue is fundamental to achieving truthful fracture toughness (G_{IIc}) from the plateau of the resistance curve (*R*-curve). In this work, a numerical analysis was performed using a CZM on the ENF and ELS specimen geometries. This approach allows the simulation of damage initiation and growth, thus providing an appropriate method to assess the influence of the specimen dimensions and material properties on the measured G_{IIc}. The simulations focus on the assessment of the effect of initial crack length, fracture toughness and local strength on the fracture toughness measurements.

DATA-REDUCTION SCHEME

Classical methods

The classical data-reduction schemes used to determine the fracture energy in mode II are usually based on the specimen compliance calibration or on the beam theory. The CCM is based on the Irwin–Kies equation:

$$G_{II} = \frac{P^2}{2B}\frac{dC}{da} \tag{1}$$

which depends on the compliance ($C = \delta/P$) calibration as a function of the crack length a. The most used data-reduction scheme is the CBT,[21]

$$G_{\mathrm{II}} = \begin{cases} \dfrac{9\,P^2\,(a\,+\,|\Delta_{\mathrm{II}}|)^2}{16B^2h^3E_{\mathrm{L}}} & \text{(ENF)} \\ \dfrac{9\,P^2\,(a\,+\,|\Delta_{\mathrm{II}}|)^2}{4B^2h^3E_{\mathrm{L}}} & \text{(ELS)} \end{cases} \tag{2}$$

where B is the specimen width, E_{L} is the longitudinal elastic modulus and $\Delta_{\mathrm{II}} = 0.42\,\Delta_{\mathrm{I}}$ for the ENF and $\Delta_{\mathrm{II}} = 0.49\,\Delta_{\mathrm{I}}$ for the ELS, being

$$\Delta_{\mathrm{I}} = h\sqrt{\frac{E_{\mathrm{L}}}{11\,G_{\mathrm{LT}}}\left[3 - 2\left(\frac{\Gamma}{1+\Gamma}\right)^2\right]} \tag{3}$$

with,

$$\Gamma = 1.18\,\frac{\sqrt{E_{\mathrm{L}}E_{\mathrm{T}}}}{G_{\mathrm{LT}}} \tag{4}$$

where E_{T} and G_{LT} are the transverse and shear modulus, respectively (Fig. 2). Using these methods (CCM and CBT), the crack length measurement is a fundamental task to be performed during the fracture test. However, this procedure is very difficult to execute with the required accuracy. Effectively, in mode II fracture characterization tests the crack tends to close during propagation hindering a clear identification of its tip. Additionally, quasi-brittle materials develop a non-negligible FPZ in the vicinity of the crack tip, characterized by the development of toughening mechanisms leading to a softening nonlinear region. This phenomenon is responsible for energy dissipation during crack propagation and should be considered in the selected data-reduction scheme. Thus, when a is used in the calculations, the FPZ effect is not accounted for in the evaluation of G_{IIc}. Here, the equivalent crack concept is used to define a data-reduction scheme based on the specimen compliance. This method does not require crack length monitoring during its growth and accounts for the energy dissipated in the FPZ.

Compliance-based beam method

ENF

Using the Timoshenko beam theory, the specimen compliance is given by[22]

$$C = \frac{3a^3 + 2L^3}{8Bh^3E_{\mathrm{L}}} + \frac{3L}{10Bh\,G_{\mathrm{LT}}} \tag{5}$$

In the early stages of loading, the initial values of compliance C_0 and crack length a_0 can be used to estimate a corrected flexural modulus E_{f},

$$E_{\mathrm{f}} = \frac{3a_0^3 + 2L^3}{8\,B\,h^3}\left(C_0 - \frac{3L}{10\,B\,h\,G_{\mathrm{LT}}}\right)^{-1} \tag{6}$$

Table 1 Nominal elastic properties of bovine cortical bone[23]

E_{L} (GPa)	E_{T} (GPa)	G_{LT} (GPa)	ν_{LT}
20.4	11.7	4.1	0.36

This procedure is quite effective because material variability among different specimens leads to non-negligible scatter on the elastic modulus. The beam theory (Eq. 5) does not include root rotation effects and stress concentrations at the crack tip. Following this approach, the longitudinal modulus is not a measured property but a parameter estimated from C_0 and a_0, thus accounting for the above referred effects. During crack growth the current compliance C is used to estimate an equivalent crack length a_{e} through Eqs (5) and (6),

$$a_e = \left[\frac{C_{\mathrm{c}}}{C_{0_{\mathrm{c}}}}a_0^3 + \frac{2}{3}\left(\frac{C_{\mathrm{c}}}{C_{0_{\mathrm{c}}}} - 1\right)L^3\right]^{1/3} \tag{7}$$

where

$$C_{\mathrm{c}} = C - \frac{3L}{10\,B\,h\,G_{\mathrm{LT}}};\quad C_{0\mathrm{c}} = C_0 - \frac{3L}{10\,B\,h\,G_{\mathrm{LT}}} \tag{8}$$

Using Eqs (1) and (5), $G_{\mathrm{II}} = \mathrm{f}(a_{\mathrm{e}})$ can be obtained as

$$G_{\mathrm{II}} = \frac{9P^2a_{\mathrm{e}}^2}{16B^2h^3E_{\mathrm{f}}} \tag{9}$$

The R-curve can now be determined without monitoring a during propagation, which is difficult to perform accurately in this test. The only material property required is G_{LT}. However, previous studies using a wide range of values of G_{LT} revealed that it does not influence the measured G_{IIc}.[22] Consequently, a typical value (Table 1) can be used.

ELS

The compliance equation for the ELS is given by[16]

$$C = \frac{3a^3 + L^3}{2Bh^3E_{\mathrm{L}}} + \frac{3L}{5BhG_{\mathrm{LT}}} \tag{10}$$

The ELS presents an important difference relative to the ENF test. Effectively, the ELS presents two sources of variability between specimens, i.e. the E_{L} and the clamping conditions which are never perfect. Consequently, the modulus should not be estimated in the same way as in the ENF because the clamping conditions affect the measured value. Therefore, E_{L} should be measured for each specimen before performing the fracture test owing to its important scatter among different specimens.

Taking into account the initial crack length (a_0) and the corresponding initial (elastic) compliance (C_0) it can be

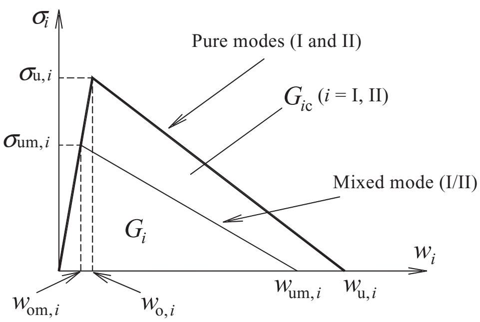

Fig. 3 Sketch of the pure (I or II) and mixed (I/II) bilinear cohesive model.

written from Eq. (10)

$$C_0 - \frac{3a_0^3}{2\,Bh^3 E_L} = \frac{L_{ef}^3}{2\,Bh^3 E_L} + \frac{3L_{ef}}{5\,BhG_{LR}} \tag{11}$$

which gives the effective length (L_{ef}) when a perfect clamping is assumed. During propagation Eq. (10) can now be rewritten as

$$C - \frac{3a_e^3}{2\,Bh^3 E_L} = \frac{L_{ef}^3}{2\,Bh^3 E_L} + \frac{3L_{ef}}{5\,BhG_{LR}} \tag{12}$$

which, accounting for Eq. (11) leads to

$$a_e = \left[(C - C_0)\frac{2Bh^3 E_L}{3} + a_0^3\right]^{1/3} \tag{13}$$

Following this methodology, a_e does not depend on L_{ef}, which constitutes an advantage, because L_{ef} depends on clamping conditions, which can vary from test to test. Combining Eqs (1) and (10), it turns

$$G_{II} = \frac{9P^2 a_e^2}{4B^2 h^3 E_L} \tag{14}$$

As in the ENF test, this approach propitiates an R-curve without monitoring a in the course of the fracture test.

NUMERICAL ANALYSIS

A cohesive mixed-mode model developed in de Moura *et al.*[22] was used to simulate damage initiation and growth. This formulation allows simulating pure-mode loading cases because they correspond to particular conditions of a more general mixed-mode loading. The model assumes a linear relationship between stresses and relative displacements in the softening region (Fig. 3). This linear softening law has proved to be adequate to simulate micro-cracking phenomenon ahead of the crack tip observed in mode II fracture characterization tests in wood.[24] A similar damage mechanism is referred to occur in mode II fracture characterization of bone,[13] which supports the choice of this law. Damage initiation is simulated by quadratic stress criterion

$$\begin{aligned} &\left(\frac{\sigma_I}{\sigma_{u,I}}\right)^2 + \left(\frac{\sigma_{II}}{\sigma_{u,II}}\right)^2 = 1 \quad && \text{if } \sigma_I \geq 0 \\ &\sigma_{II} = \sigma_{u,II} && \text{if } \sigma_I \leq 0 \end{aligned} \tag{15}$$

where σ_i (i = I, II) represent the stresses in each mode and $\sigma_{u,i}$ the respective local strengths. Crack propagation was simulated by linear energetic criterion

$$\frac{G_I}{G_{Ic}} + \frac{G_{II}}{G_{IIc}} = 1 \tag{16}$$

From Fig. 3 it is shown that the small triangle area corresponds to the energy dissipated in each mode (G_i) and the biggest one to the respective toughness (G_{ic}). More details are given in de Moura *et al.*[22]

A two-dimensional analysis was implemented in ABAQUS® software using 7680 isoparametric plane stress 8-node solid elements. Two hundred forty 6-node cohesive elements were disposed at the specimens half-height along direction x (Fig. 4), allowing the simulation of damage initiation and growth. These elements are

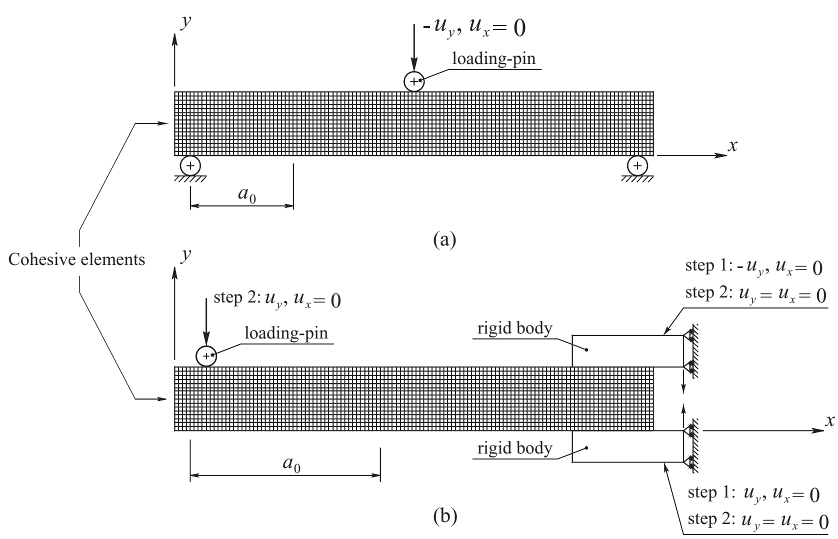

Fig. 4 Meshes used in the ENF (a) and ELS (b) specimens simulation.

Table 2 Range of the cohesive properties used in the simulations

G_{IIc} (N mm^{-1})	$\sigma_{u,II}$ (MPa)
3–7	30–50

compatible with the 8-node isoparametric solid elements and were implemented through the user subroutine option available in ABAQUS®. Along the pre-crack the cohesive elements were considered 'opened', which means that they were only able to transmit normal compressive stresses, avoiding spurious interpenetrations. The friction effects at the pre-crack were neglected, because it was observed in previous studies that contact is confined to the loading regions.[25] Moreover, in the experiments the use of two Teflon® films with a pellicle of lubricator between them will drastically diminish this effect.[24] Refined meshes (Fig. 4) were used to provide several points undergoing softening, thus contributing to smooth damage growth and mesh independent results. Loading and supporting devices (Fig. 2) were simulated as rigid bodies and contact conditions assumed to prevent interpenetration. Clamping in the ELS (Fig. 4b) was simulated by two rigid blocks that tighten the specimen. Different amounts of tightening were considered (step 1 in Fig. 4b) to verify their influence on the measured G_{IIc}. Friction coefficient of 0.25 for the contact pair bone/steel[26] was considered in this support. Fracture simulations (material elastic properties in Table 1) were performed imposing the displacement u_y (step 2 in Fig. 4b) to the loading pin considering the TL fracture system (Figs 1 & 2). Small displacement increments (0.1% $\times$ δ) were considered to provide stable crack growth and a nonlinear geometrical analysis was carried out.

RESULTS

The objective of this work is to verify which conditions must be fulfilled to provide accurate measurements of G_{IIc} using the ENF and ELS tests. Consequently, typical G_{IIc} and $\sigma_{u,II}$ limiting values were assumed in the simulations (Table 2). The maximum specimen length that can be obtained from the bovine femur (Fig. 1) is in the order of 60–70 mm. Because the ENF test is more susceptible to the specimen length than the ELS (see discussion below), it was decided to use 70 mm for the ENF and 60 mm for the ELS test. The specimens' height ($2h$) and width (B) were set equal to 8 and 3 mm, respectively.

ENF

The ENF test can lead to unstable crack growth, namely for shorter crack lengths.[27] Consequently, in the ENF test

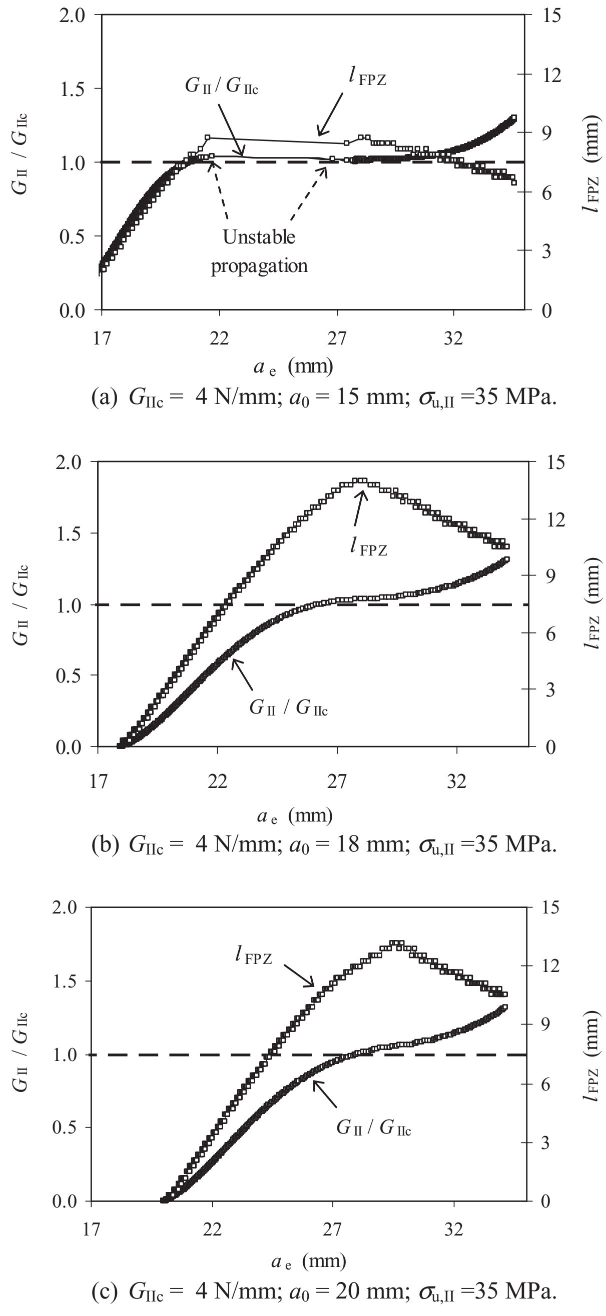

Fig. 5 Effect of the pre-crack length a_0 on the ENF test performance.

the available region for unconstrained damage growth is quite limited. In fact, during self-similar crack propagation the FPZ developed ahead of the crack tip must be maintained far from the central loading point (Fig. 2a), for a correct G_{IIc} measurement, because the compressive effects lead to a spurious toughness enhancement. This problem is aggravated for higher values of G_{IIc}, which means that a parametric study is fundamental to define

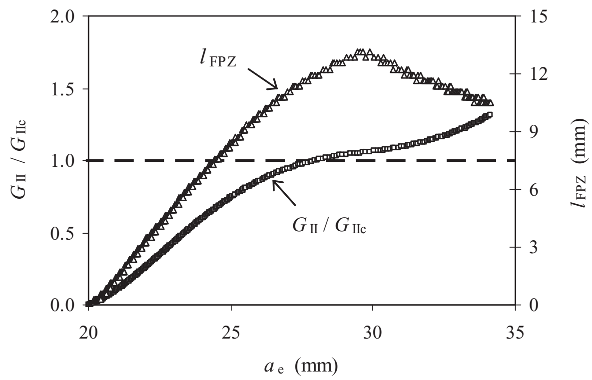

(a) G_{IIc} = 4 N/mm; a_0 = 20 mm; $\sigma_{u,II}$ =35 MPa.

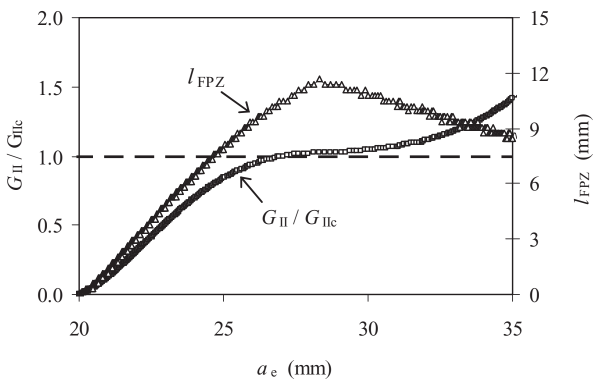

(b) G_{IIc} = 4 N/mm; a_0 = 20 mm; $\sigma_{u,II}$ =40 MPa.

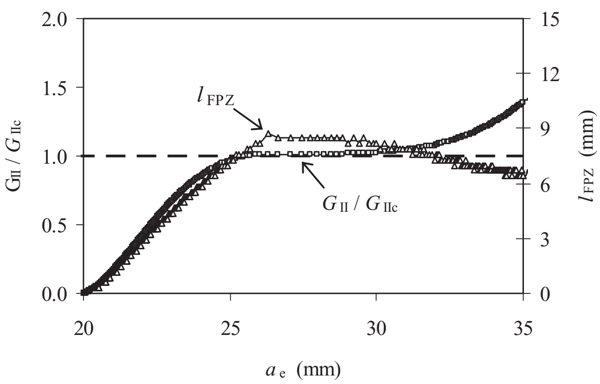

(c) G_{IIc} = 4 N/mm; a_0 = 20 mm; $\sigma_{u,II}$ =50 MPa.

Fig. 6 Effect of the local strength $\sigma_{u,II}$ on the ENF test performance.

the application limits of the ENF test. The local strength ($\sigma_{u,II}$ in Fig. 3) also plays an important role in this context. Effectively, lower values of $\sigma_{u,II}$ increase the tail of the softening region for a given toughness (i.e. area of the biggest triangle in Fig. 3) thus contributing to increase the FPZ size. A similar effect occurs when, for a given $\sigma_{u,II}$, higher values of toughness are considered.

The first parameter to be analysed is the pre-crack length, a_0, considering a useful specimen length $2L$ = 65 mm (Fig. 2a). Figure 5 presents the *R*-curves (Eq. 9) and the corresponding FPZ length (l_{FPZ}) as a function of a_e (Eq. 7), for three different values of a_0. The strain energy release rate was normalized by its toughness value (G_{IIc} = 4 N mm^{-1}) which means that the inputted value is well captured if the obtained ratio points to the unity. From Fig. 5a it can be verified that unstable propagation occurs for the lowest pre-crack length, $a_0 = 15$ mm. For the other crack lengths, stable propagation took place although the plateau corresponding to self-similar crack growth has become shorter, and practically does not exist for a_0 = 20 mm (Fig. 5c). The explanation for this occurrence is related to compression effects near the central loading point affecting the FPZ development. Effectively, those effects come out earlier as a_0 increases. This consequence can be clearly verified by the pronounced decrease of the FPZ length (l_{FPZ}) after a quite short plateau, thus showing the spurious effect induced by the central loading.

The influence of the local strength which defines the maximum stress that the material can attain at the crack tip ($\sigma_{u,II}$ in Fig. 3) was also assessed. From Fig. 6 it can be observed that the size of the plateau region of the *R*-curves increases with the enhancement of $\sigma_{u,II}$, considering the same toughness (G_{IIc} = 4 N mm^{-1}), i.e. the same triangular area (Fig. 3). This is a consistent result owing to the decrease of the critical displacement corresponding to the complete failure observed on the triangular cohesive law, $w_{u,II}$. For $\sigma_{u,II}$ = 50 MPa (Fig. 6c), the plotting of l_{FPZ} as a function of a_e shows an important plateau, thus revealing self-similar crack growth conditions for a remarkable length. The used values (35–50 MPa) represent a rather conservative range because in Turner *et al.*[28] values ranging between 50.4 and 51.6 MPa are measured for human bone which has inferior properties than bovine. This means that more favourable conditions (i.e. higher local strengths) are expected to exist in the experiments.

The performance of the ENF test for different values of toughness was also analysed. Feng[2] evaluated the G_{IIc} of bovine bone as being equal to 2.43 ± 0.836 N mm^{-1}. In order to have a conservative analysis it was decided to consider values of G_{IIc} ranging from 4 to 7 N mm^{-1}, because the described spurious effects become more important with increasing values of G_{IIc}. This means that the selected range of G_{IIc} (i.e. 4–7 N mm^{-1}) is more demanding in defining the specimen geometry, than the value pointed by Feng.[2] Figure 7 presents the *R*-curves for three different values of G_{IIc} (5, 6 and 7 N mm^{-1}) considering $\sigma_{u,II}$ = 50 MPa and a_0 = 20 mm, which were also used in Fig. 6c with G_{IIc} = 4 N mm^{-1}. Thus, from Figs 6c and 7a–c, it can be verified that the plateau length of the *R*-curves diminishes as the G_{IIc} increases, which is a logical trend. In reality, the toughness enhancement

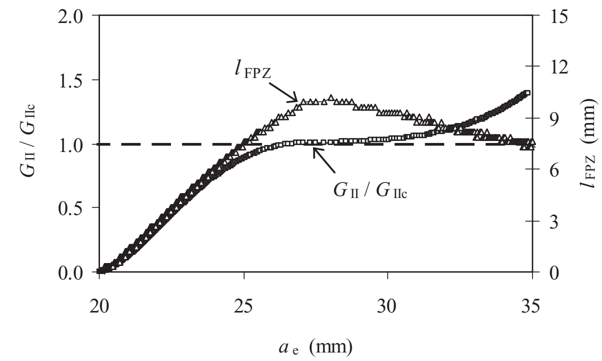

(a) G_{IIc} = 5 N/mm; a_0 = 20 mm; $\sigma_{u,II}$ =50 MPa.

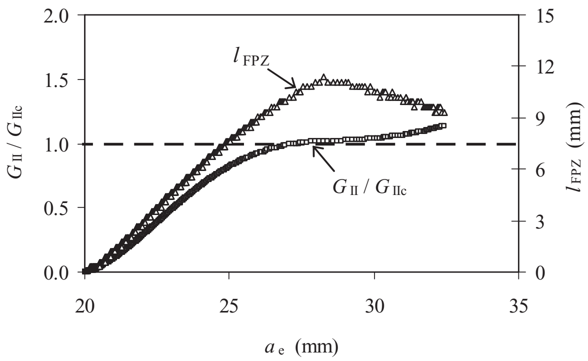

(b) G_{IIc} = 6 N/mm; a_0 = 20 mm; $\sigma_{u,II}$ =50 MPa.

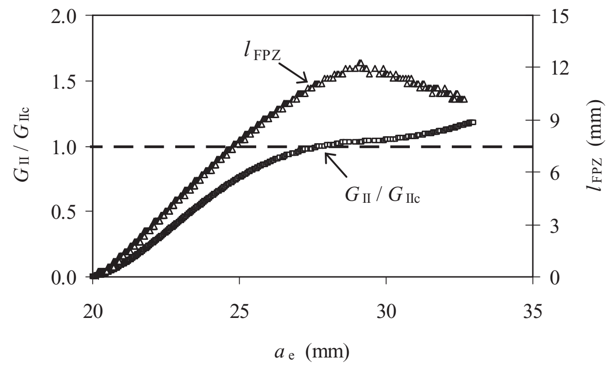

(c) G_{IIc} = 7 N/mm; a_0 = 20 mm; $\sigma_{u,II}$ =50 MPa.

Fig. 7 Effect of the toughness on the ENF test performance.

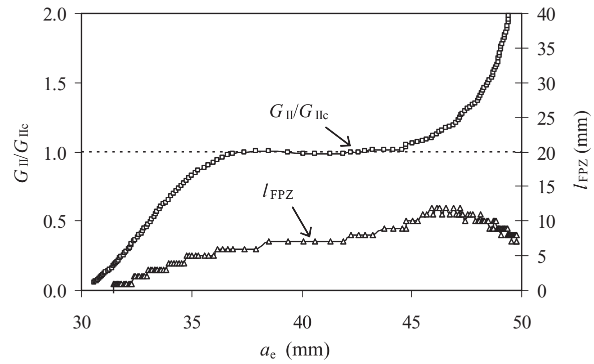

(a) G_{IIc} = 7 N/mm; a_0 = 30 mm; δ_c=0.1 mm.

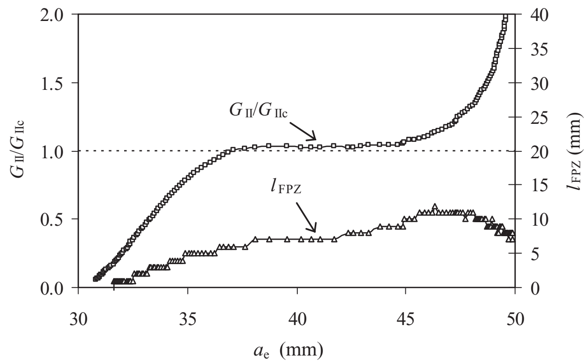

(b) G_{IIc} = 7 N/mm; a_0 = 30 mm; δ_c=0.07 mm.

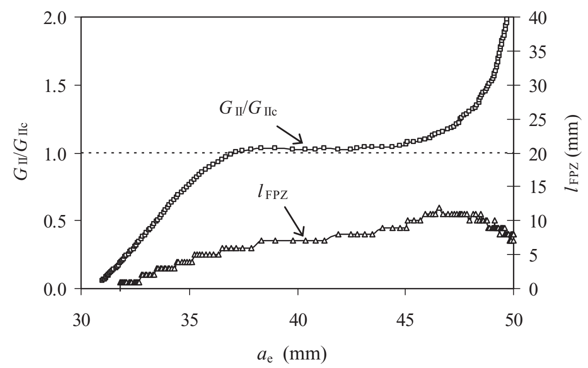

(c) G_{IIc} = 7 N/mm; a_0 = 30 mm; δ_c=0.05 mm.

Fig. 8 Effect of the clamping conditions on the ELS test performance.

leads to an increase of the tail corresponding to the softening region of the triangular law when $\sigma_{u,II}$ is kept constant (Fig. 3), which reflects on higher values of l_{FPZ}. Consequently, the FPZ is affected prematurely by the central loading P, thus leading to shorter plateaus, both on the R-curves and on the l_{FPZ} = f(a_e) (Figs 6c & 7a–c).

In conclusion, it can be affirmed that a specimen with a total and useful lengths ($2L_1$ and $2L$) of 70 and 65 mm, respectively, with a pre-crack (a_0) of 20 mm (Fig. 2a) provides satisfactory conditions to perform the mode II toughness (G_{IIc}) measurements in cortical bovine bone using the ENF test. This conclusion is based on a parametric analysis considering a range of fracture parameters (i.e. $\sigma_{u,II}$ and G_{IIc}) which can be considered pessimistic in which concerns the arise of the spurious effects.

ELS

The ELS test presents a longer length relative to the ENF case for crack growing, which is advantageous considering the discussed problems affecting the self-similar crack growth. Owing to this less restrictive condition, specimens of global length of 60 mm (L_1 in Fig. 2b) were used because they are easier to obtain than the ones of 70 mm. The useful specimen length (L) was set equal to 48 mm, because the load was applied 4 mm far from the specimen edge (d) and 8 mm was used for clamping embedment. The a_0 was assumed to be 30 mm to provide stable crack propagation conditions. However, in the ELS test the clamping conditions also require a parametric study. In fact, they depend on the tightening load exerted on the clamped region. To evaluate this effect three different tights (opposite displacements of 0.1, 0.07 and 0.05 mm applied to each clamping block (Fig. 2b)) were simulated, considering the limiting values of cohesive parameters used in the simulations of the ENF test: $\sigma_{u,II} = 50$ MPa and $G_{IIc} = 7$ N mm^{-1} (Fig. 7c). From Fig. 8a it can be observed that a perfect reproduction of the inputted value is attained, although the compressive stresses at clamping obtained in FEM computations (220 MPa) overcome the compressive strength of the bovine bone (a value of 146 MPa is presented in Chen *et al.*[29]). In Fig. 8b and c it is observed that overestimation errors of 2–3% on G_{IIc} are obtained with compressive stresses of 150 and 110 MPa at the clamped region, respectively.

The numerical analysis of the ELS test shows that a specimen with total and useful lengths (L_1 and L) of 60 and 48 mm, respectively, with a pre-crack length (a_0) of 30 mm (Fig. 2b) is appropriate. The clamping force is limited by the bone compressive strength, and a tightening of 0.05 mm applied to each clamping block should be used. These conditions provide satisfactory measurements of mode II toughness (G_{IIc}) in cortical bovine bone using the ELS test. Once again, this conclusion is based on fracture parameters (i.e. $\sigma_{u,II}$ and G_{IIc}) which can be considered pessimistic, taking into account the typical values found in the literature.

CONCLUSIONS

The ENF and the ELS tests were numerically analysed in order to verify their applicability to characterize the bovine bone fracture under mode II loading. The numerical analyses were used to estimate the sensitivity of each test to the initial crack length, local strength, toughness and clamping conditions. A data-reduction scheme based on the specimen compliance and the crack equivalent concept was used to overcome the difficulties inherent to crack monitoring during its growth. A cohesive damage model was used to simulate damage initiation and propagation, thus assessing the influence of several parameters on the measured G_{IIc} and the efficacy of the proposed data-reduction scheme. The effects of initial crack length, local strength and toughness were analysed in order to verify their influence on the measured G_{IIc} relative to the inputted value. The present study allows identifying the limiting aspects of each test and to optimize the geometry leading to a correct estimation of the bovine bone properties under mode II loading. The critical aspect of the ENF test is related to the eventual spurious effect induced by central loading on the measured G_{IIc}. In the ELS case special attention should be dedicated to the clamping conditions that can also affect the measured toughness values. However, the main finding of the presented work is that with careful geometry selection, good estimations of G_{IIc} can be provided by both tests. It should be noted that pessimistic values for σ_{uII} and G_{IIc} concerning the rise of spurious effects have been considered in the numerical analysis. This means that it is expectable that real conditions (i.e. higher values of σ_{uII} and lower values of G_{IIc}) will propitiate even better performances for the selected geometries. This work can be considered a fundamental step in the study of the mode II fracture of bone, because proposed testing geometries until now cannot be considered appropriate solutions.

Acknowledgement

The authors thank the Portuguese Foundation for Science and Technology for supporting the work here presented, through the research project PDTC/EME-PME/71273/2006.

REFERENCES

1 Currey, J. D., Brear, K., Zioupos, P. and Reilly, G. C. (1995) Effect of formaldehyde fixation on some mechanical properties of bovine bone. *Biomaterials* **16,** 1267–1271.
2 Feng, Z., Rho, J., Han, S. and Ziv, I. (2000) Orientation and loading condition dependence of fracture toughness in cortical bone. *Mat. Sci. Eng. C – Bio. S.* **11,** 41–46.
3 Norman, T. L., Vashishtht, D. and Burr, D. B. (1995) Fracture toughness of human bone under tension. *J. Biomech.* **28,** 309–320.
4 Vashishth, D., Behiri, J. C. and Bonfield, W. (1997) Crack growth resistance in cortical bone. Concept of microcrack toughening. *J. Biomech.* **30,** 763–769.
5 Zioupos, P. (1998) Recent developments in the study of failure of solid biomaterials and bone: 'fracture' and 'pre-fracture' toughness. *Mat. Sci. Eng. C – Bio. S.* **6,** 33–40.
6 Nalla, R. K., Kruzic, J. J., Kinney, J. H. and Ritchie, R. O. (2004) Effect of aging on the toughness of human cortical bone: evaluation by R-curves. *Bone* **35,** 1240–1246.
7 Ritchie, R. O., Kinney, J. H., Kruzic, J. J. and Nalla R. K. (2005) A fracture mechanics and mechanistic approach to the failure of cortical bone. *Fatigue Fract. Engng. Mater. Struct.* **28,** 345–371.

8 Yan, J., Mecholsky Jr., J. J. and Clifton, K. B. (2007) How tough is bone? Application of elastic–plastic fracture mechanics to bone. *Bone* **40,** 479–484.
9 Yang, Q. D., Cox, B. N., Nalla, R. K. and Ritchie, R. O. (2006) Re-evaluating the toughness of human cortical bone. *Bone* **38,** 878–887.
10 Ural, A. and Vashishth, D. (2006) Cohesive finite element modelling of age-related toughness loss in human cortical bone. *J. Biomech.* **39,** 2974–2982.
11 Phelps, J. B., Hubbard, G. B., Wang, X. and Agrawal, C. M. (2000) Microstructural heterogeneity and the fracture toughness of bone. *J. Biomed. Mater. Res.* **51,** 735–741.
12 Wang, X., Lankford, J. and Agrawal, C. M. (1994) Use of a compact sandwich specimen to evaluate fracture toughness and interfacial bonding of bone. *J. Appl. Biomater.* **5,** 315–323.
13 Norman, T. L., Nivargikar, V. and Burr, D. B. (1996) Resistance to crack growth in human cortical bone is greater in shear than in tension. *J. Biomech.* **29,** 1023–1031.
14 Brown, C. U., Yeni, Y. N. and Norman, T. L. (2000) Fracture toughness is dependent on bone location – a study of the femoral neck, femoral shaft, and the tibial shaft. *J. Biomed. Mater. Res.* **49,** 380–389.
15 Catanese III, J., Iverson, E. P., Ng, R. K. and Keaveny, T. M. (1999) Heterogeinity of mechanical properties of demineralized bone. *J. Biomech.* **32,** 1365–1369.
16 Silva, M. A. L., Morais, J. J. L., de Moura, M. F. S. F. and Lousada, J. L. (2007) Mode II wood fracture characterization using the ELS test. *Eng. Fract. Mech.* **74,** 2133–2147.
17 Yoshihara, H. and Satoh, A. (2009) Shear and crack tip deformation correction for the double cantilever beam and three-point end-notched flexure specimen for mode I and mode II fracture toughness measurement of wood. *Eng. Fract. Mech.* **76,** 335–346.
18 de Moura, M. F. S. F. and de Morais, A. B. (2008) Equivalent crack based analysis of ENF and ELS tests. *Eng. Fract. Mech.* **75,** 2584–2596.
19 de Moura, M. F. S. F., Campilho, R. D. S. G. and Gonçalves, J. P. M. (2009) Pure mode II fracture characterization composite bounded joints. *Int. J. Solids Struct.* **46,** 1589–1595.
20 Blackman, B. R. K., Kinloch, A. J. and Paraschi, M. (2005) The determination of the mode II adhesive fracture resistance, GIIc, of structural adhesive joints: an effective crack length approach. *Eng. Fract. Mech.* **72,** 877–897.
21 Wang, Y. and Williams, J. G. (1992) Corrections for mode II fracture toughness specimens of composite materials. *Compos. Sci. Technol.* **43,** 251–256.
22 de Moura, M. F. S. F., Silva, M. A. L., de Morais, A. B. and Morais, J. J. L. (2006) Equivalent crack based mode II fracture characterization of wood. *Eng. Fract. Mech.* **73,** 978–993.
23 Martin, R. B., Burr, D. B. and Sharkey, N. A. (1998) *Skeletal Tissue Mechanics*, ISBN 0-387-98474-7. Springer-Verlag, New York.
24 de Moura, M. F. S. F., Silva, M. A. L., Morais, J. J. L., de Morais, A. B. and Lousada, J. J. L. (2009) Data reduction scheme for measuring G_{IIc} of wood in End-Notched Flexure (ENF) tests. *Holzforschung* **63,** 99–106.
25 Silva, M. A. L., de Moura, M. F. S. F. and Morais, J. J. L. (2006) Numerical analysis of the ENF test for mode II wood fracture. *Compos. Part A – Appl. S.* **37,** 1334–1344.
26 Davim, J. P. and Marques, N. (2004) Dynamical experimental study of friction and wear behaviour of bovine cancellous bone sliding against a metallic counterface in a water lubricated environment. *J. Mater. Process. Tech.* **152,** 389–394.
27 Carlsson, L. A., Gillespie, J. W. and Pipes, R. B. (1986) On the analysis and design of the end notched flexure (ENF) specimen for mode II testing. *J. Comp. Mat.* **20,** 594–604.
28 Turner, C. H., Wang, T. and Burr, D. B. (2001) Shear strength and fatigue properties of human cortical bone determined from pure shear tests. *Calcified Tissue Int.* **69,** 373–378.
29 Chen, P. Y., Stokes, A. G. and McKittrick, J. (2009) Comparison of the structure and mechanical properties of bovine femur bone and antler of the North American elk (Cervus elaphus canadensis). *Acta Biomater.* **5,** 693–706.